Military Technical College
Kobry El-Kobbah,
Cairo, Egypt.

13th International Conference on Applied Mechanics and Mechanical Engineering.

THE EFFECT OF DROPLETS ON BUOYANCY IN VERY RICH ISO-OCTANE-AIR FLAMES

SULAIMAN* S.A. and LAWES** M.

ABSTRACT

An experimental study is performed with the aim of investigating the effect of the presence of droplets in flames of very rich iso-octane-air mixture under normal gravity. Experiments are conducted for initial pressures in the range 100-160 kPa and initial temperatures 287-303 K at an equivalence ratio of 2.0. Iso-octane-air aerosols are generated by expansion of the gaseous pre-mixture (condensation technique) to produce a homogeneously distributed suspension of near mono-disperse fuel droplets. The droplet size varies with time during expansion; hence the effect of droplet size in relation to the cellular structure of the flame is investigated by varying the ignition timing. Flame propagation behavior is observed in a cylindrical vessel equipped with optical windows by using schlieren photography. Local flame speeds are measured to assess the effect of buoyancy in gaseous and aerosol flames. It is found that the presence of droplets results in a much earlier onset of instabilities, at a rate faster than that taken for the buoyancy effect to take place. Flame instabilities, characterised by wrinkling and cellular surface structure, increase the burning rate due to the associated increase in surface area. Consequently, the presence of droplets results in a faster flame propagation rate than that displayed by a gaseous flame. The mechanism of flame instabilities that causes a significant reduction of the buoyancy effect is discussed.

KEY WORDS

Buoyancy, Combustion, Droplets, Flame, Instabilities

* Senior Lecturer, Dept. of Mech. Eng., Universiti Teknologi Petronas, Malaysia.
** Senior Lecturer, School of Mech. Eng., University of Leeds, United Kingdom.

INTRODUCTION

The combustion of clouds of fuel droplets is of practical importance in engines, furnaces and also for prevention of explosion and fire in the storage and use of fuels. Theoretical [1] and experimental [2-4] evidence suggests that flame propagation through clouds of droplets, under certain circumstances, is higher than that in a fully vaporized homogeneous mixture. Even though this may be advantageous in giving more rapid burning, its effects on emissions are uncertain.

Most combustion in engineering applications takes place under turbulent conditions. Nevertheless, it is well established that the laminar burning rate plays an important role in turbulent combustion [5]. Information on laminar burning velocity is sparse, even for gaseous mixtures at conditions pertaining to engines, which range from sub-atmospheric to high pressure and temperature. Such data for fuel sprays and for gas-liquid co-burning [6-8] are even sparser than for gases. As a consequence, there is little experimental data of a fundamental nature that clearly demonstrates the similarities and differences in burning rate, either laminar or turbulent, between single and two phase combustion.

In the present work, the influence of droplets in iso-octane-air mixtures within the upper flammability limit (rich) is investigated. Such gaseous mixtures are well known, from a number of previous works, for example in [9-11], to experience the effect of buoyancy or natural convection during combustion. Some of the previous studies were performed in tubes. However, Andrews and Bradley [12] suggested that the limit of flammability obtained by the tube method would be subjected to the same sources of error [13] as would be the burning velocity measurements using tubes, mainly due to wall quenching. Thus studies in larger tube diameters or in large explosion vessels have been recommended.

Figure 1 shows an illustration of two centrally ignited spherical flames to describe the effect of buoyancy [14]. The open arrow represents the local velocity resulted from gas expansion during flame propagation. The solid arrow, which points upward, represents the local velocity caused by the buoyancy or natural convection effect. The dashed lines show the resulting flame front accounting for the net velocity. With the absence of the buoyancy effect, the resulting flame would be spherical or circular when viewed from the side. However, with the presence of the buoyancy effect, the resulting flame has a flatter bottom surface as that illustrated in Fig. 1.

EXPERIMENTAL APPARATUS AND TECHNIQUES

Figure 2 shows the photograph and schematic of the aerosol combustion apparatus. The combustion vessel, which essentially resembled a Wilson cloud chamber [15], was a cylindrical vessel of 305 mm diameter by 305 mm long (internal dimensions), with a working volume of 23.2 litres. On both end plates of the combustion vessel circular optical access windows of 150 mm diameter were provided for characterization of aerosol and photography of flame propagation. To initially mix the reactants four fans, driven by electric motors, were mounted adjacent to the wall of the vessel. Two electrical heaters were attached to the wall of the vessel to preheat the vessel and mixture to 303 K. The expansion vessel, which has a volume of 28 litres, was connected to the combustion vessel by an interconnecting pipe through a port. The

vacuum pump, indicated in Fig. 2 (a), was used to evacuate the system and to remove particulates prior to preparation of the mixture.

The aerosol mixtures were prepared by a condensation technique, which generated near mono-dispersed droplet suspensions. This was achieved by controlled expansion of a gaseous fuel-air mixture from the combustion vessel into the expansion vessel that was pre-evacuated to less than 1 kPa. The expansion caused a reduction in the pressure and temperature of the mixture, which took it into the condensation regime and caused droplets to be formed.

The characteristics of the generated aerosol were calibrated by in-situ measurements of the temporal distribution of pressure, temperature, and droplet size and number, without combustion, with reference to the time from start of expansion. The diameters of individual droplets were measured using a Phase Doppler Anemometer (PDA) system, from which the droplet mean diameter, D_{10}, was obtained. Since the expansion took place over a period of several seconds while combustion took place over less than 100 ms, the far field values of D_{10} were assumed to be constant during combustion.

The mean droplet diameter varied with time during expansion; hence the effect of droplet size in relation to the cellular structure of the flame was investigated by varying the ignition timing. The iso-octane-air mixture was ignited at the centre of the combustion vessel by an electric spark of approximately 500 mJ. The flame front was monitored through the vessel's windows by schlieren movies, which were recorded using a high-speed digital camera at a rate of 1000 frames per second and with a resolution of 512 $\times$ 512 pixels. The flame image was processed digitally by using image-processing software to obtain the flame radius. The velocity of the flame front, also known as the stretched flame speed, S_n, is obtained directly from the measured flame front radius, r, by

$$S_n = \frac{dr}{dt} \tag{1}$$

Similarly, the local flame speed is given by

$$S_L = \frac{dL}{dt} \tag{2}$$

where L is the distance between the local flame front and the spark electrode as measured from the schlieren image of the flame.

RESULTS AND DISCUSSIONS

Figure 3 shows the schlieren photographs of flames at maximum viewable radius and the corresponding contour plots at 2 ms intervals for a gaseous and also aerosol mixtures. The mixtures were initially at ϕ_{ov} = 2.0, temperatures between 287 and 303 K, and pressures between 100 and 159 kPa. For the aerosol mixtures, the droplet mean diameters, D_{10}, were 5 μm and 13 μm. It must be noted that the relatively small differences in pressure and temperature between the conditions in the three images has been shown, for gaseous flames, to have little effect on the flame structure [16].

Hence, it is assumed that the difference in the flame structure is entirely due to the effects of droplets. In Fig. 3(a), the image is slightly darker than the others due to low exposure setting of the camera. The circular black areas at the corners of the photographs represent the region beyond the window of the combustion vessel. The electrode holder and thermocouple are clearly shown on the middle-right section in each photograph.

It is shown in the schlieren image in Fig. 3(a) that for gaseous flame, the upward distance of the flame propagation is greater than the downward one, which is a sign of the buoyancy effect as described for Fig. 2. The upper surface of the gaseous flame is relatively smoother and has fewer cells as compared to the lower surface. In the contour plot for the gaseous flame in Fig. 3(a), larger spacing between flame contours is shown for the upper propagation as compared to the lower one. This suggests faster upward flame propagation than the downward propagation. Conversely, the difference between the leftward and rightward propagations is shown to be small, the rightward propagation being very close to the flame radius. Hence it is shown that significant difference in propagation rate occurs only in the vertical direction.

With the presence of droplets of 5 μm, it is shown in Fig. 3(b) that trend of vertical flame propagation is almost similar to that for the gaseous flame in Fig 3(a). However the aerosol flame has more cells on its surface than the gaseous one. Interestingly, with bigger droplets (D_{10} = 13 μm), it is shown in Fig. 3(c) that the resulting flame is highly cellular. The contour plot of the flame shows faster burning rate (large spacing between contours) and also smaller difference between the upward and downward propagation rate (more uniform contour spacing in all directions) as compared to those in Figs. 3 (a) and (b). Hence it is suggested that with the presence of large diameter droplets, the buoyancy effect demonstrated in gaseous flames of rich mixtures is overcome by instabilities and consequently faster burning rate, such that there was less time available for natural convection to be significant.

Figure 4 shows graphs displaying the temporal variations of the flame radius and local vertical and horizontal propagation distances (from the electrode) for the gaseous iso-octane-air flame depicted in Fig. 3(a) and for the aerosol flame in Fig. 3(c), both at ϕ_{ov} = 2.0. Here the effect of the presence of large droplets (D_{10} = 13 μm) is presented. The upward, downward, leftward and rightward propagation distances between the spark gap and the corresponding flame edge were measured at 1 ms interval.

It is shown in the graph in Fig. 4(a) that for the gaseous flame, the upward propagation distance of the flame propagation is always greater than that of the downward one. In addition, the upward distance of the flame propagation increases at a steady rate, whereas the downward one decelerates; these indicate the effect of buoyancy force acting on the hot flame kernel. The difference between the leftward and rightward propagations is shown to be small, although the rightward propagation distance seems to be slightly different from the flame radius. Obviously, the flame radius and horizontal propagation distances are shown to be at approximately midway between the upward and downward components. The deceleration in the downward propagation is only experienced by the gaseous flame, as shown in Fig. 4(a). Hence, the cellularity on the bottom half of the gaseous flame in Fig. 3(a) is probably caused by hydrodynamic instabilities, as a result of an upward flow of unburned gas which velocity exceeded the flame speed at the base of the flame, as illustrated in Fig. 2. Conversely, the smoother

upper surface of the flame is probably due to flame stabilization as a result of high stretch rate. This occurs when the expanding flame front propagates through a velocity gradient in the unburned gas that is induced by the upward, buoyant acceleration of hot products as explained by Andrews and Bradley [12].

With the presence of large enough droplets (D_{10} = 13 μm), the aerosol flame burned faster than the gaseous flame. This is shown in Fig 4(b), in which the aerosol flame took approximately 60 ms to reach a radius of 50 mm, as compared to about 90 ms for the gaseous flame to reach the same radius. This is very likely caused by earlier instabilities in the aerosol flames, as depicted in Fig. 3, which promotes a faster burning rate due to increase in the flame surface area. In relation to the buoyancy, it is shown in Fig. 4(b) that such effect is absent, as implied by the gap between the upward and downward flame propagation that is significantly and consistently smaller as compared to that for the gaseous flame. Furthermore, the aerosol flame exhibits acceleration in the downward propagation as compared to deceleration in the gaseous flame.

Figure 5 shows the vertical components of the flame propagation distance from the spark electrode for the gaseous flame and also the aerosol flames (D_{10} values of 5, 13, and 16 μm) at initial conditions similar to those described for Fig. 3. The negative values indicate the downward flame propagation distances. The propagation rates for the fine aerosol (D_{10} = 5 μm) flames are shown in Fig. 5 to be similar to those for the gaseous flames, as indicated by their nearly identical curve plots, particularly for the downward propagation of the flame. In addition, the buoyancy effect is evident by the greater values of the positive distance as compared to the negative distance. It is clear in Fig. 5 that the flames within aerosols of large droplets (13 and 16 μm) propagate at a faster rate than those of fine droplets (5 μm) and gaseous. For these aerosol flames, the effect of buoyancy is not obvious. Interestingly, it is shown that the curves for upward propagation for all values of D_{10} are coincident for approximately the first 25 ms of propagation; a similar trend is observed for downward propagation up to about 16 ms. This was probably because the buoyancy is not yet in effect during those periods of initial flame kernel growth.

Figure 6 shows graphs of variation in the local flame speed (deduced by time derivative of the graphs in Fig. 4) with time from the start of ignition. The speed for the upward propagating flame is represented by the diamond markers, and the bottom one by the square markers. The circle and triangle markers represent the rightward and leftward flames respectively. The gaseous flame is shown in Fig. 6(a) to propagate faster in the upward component by about 0.4 m/s, as compared to that of the downward component, which also decreases towards a near zero value throughout propagation. A negative downward component, if were to occur, would implicate an upward flow of unburned gas at the central base of the flame; such cases were reported elsewhere; e.g. in [9], but this is beyond the scope of the present work. The sideway components of the flame speed are shown in Fig. 6(a) to be similar, which suggest the independencies of these components from the natural convection effect in the gaseous flame. With droplets (D_{10} = 13 μm), it is shown in Fig. 6(b) that all the components of flame speed nearly coincide with each other, indicating a more uniform distribution of flame speed throughout the flame surface, and hence evident the absence of the natural convection effect. However, after about 35 ms from the start of ignition, the curve for the upward component of the flame started to burn at a significantly faster rate than the other components. The reason for this is not clear and thus further investigation is required.

The mechanism of flame instabilities, which cause increased cellularity and insignificance of the buoyancy effect, in aerosol flames is probably related to the heat loss from the flame and local rapid expansion through droplet evaporation. Although droplet evaporation can also cause high gradients in the mixture strength (variations in local equivalence ratio), which might have an effect on the flame, this was negated experimentally [17] using water aerosol in propane-air mixtures. In another study [18] using a rig similar to that of the present work, it was shown that the presence of 30 μm diameter hollow spherical glass beads (no evaporation) in a gaseous iso-octane-air mixture did not alter the smooth characteristics of the flame structure as well as the burning rate. Thus it is evident that the presence of droplets probably plays an important role in the introduction of instabilities due to evaporation.

CONCLUSIONS

The effects of the presence of near mono-dispersed droplets in flames of very rich iso-octane-air mixture (ϕ_{ov} = 2.0) were investigated experimentally in a spherical explosion vessel at near atmospheric conditions. The fuel droplets, which were in the form of aerosols/vapor, were generated by condensation of the gaseous pre-mixture through expansion and this resulted in a homogeneously distributed suspension of near mono-disperse fuel droplets. The effects of droplet size in relation to the structure of the flame surface and to the burning rate were investigated by varying the ignition timing, as the droplet size varied with time during expansion. Observations of the gaseous flame using schlieren photography through the vessel's windows revealed the buoyancy effect, with distinct differences in flame surface structure and local burning rates between the upper and lower halves of the flame, similar to those described in previous studies. The presence of fine droplets (5 μm) did not cause significant change with respect to the gaseous flame in terms of the buoyancy effect, flame structure and burning rate. However, with larger droplets (13 μm) the flame became fully cellular at a faster rate and more importantly the effect of buoyancy was significantly reduced. The increased propensity to instability results in the burning rate of aerosol mixtures being faster than those in the gaseous phase at similar conditions. This is so, although the fundamental unstretched laminar burning velocity is probably unchanged by the presence of droplets.

ACKNOWLEDGMENTS

The financial support by Universiti Teknologi Petronas, Malaysia, for the experiment work at the University of Leeds, UK, is gratefully acknowledged.

REFERENCES

[1] J. B. Greenberg, "Propagation and Extinction of an Unsteady Spherical Spray Flame Front," Combust. Theory Modelling, vol. 7, pp. 163-174, 2003.

[2] D. R. Ballal and A. H. Lefebvre, "Flame Propagation in Heterogeneous Mixtures of Fuel Droplets, Fuel Vapor and Air," Proc. Combust. Inst., 1981.

[3] G. D. Myers and A. H. Lefebvre, "Propagation in Heterogeneous Mixtures of Fuel Drops and Air," Combustion and Flame, vol. 66, pp. 193-210, 1986.
[4] G. A. Richards and A. H. Lefebvre, "Turbulent Flame Speeds of Hydrocarbon Fuel Droplets in Air," Combustion and Flame, vol. 78, pp. 299-307, 1989.
[5] D. Bradley, A. K. C. Lau, and M. Lawes, "Flame Stretch Rate as a Determinant of Turbulent Burning Velocity," Phil. Trans. R. Soc. Series A, vol. 338, pp. 359, 1992.
[6] Y. Mizutani and A. Nakajima, "Combustion of Fuel Vapour-Drop-Air Systems: Part I, Open Burner Flames," Combustion and Flame, vol. 20, pp. 343-350, 1973.
[7] Y. Mizutani and A. Nakajima, "Combustion of Fuel Vapour-Drop-Air Systems: Part II, Spherical Flames in a Vessel," Combustion and Flame, vol. 21, pp. 351-357, 1973.
[8] F. Akamatsu, K. Nakabe, Y. Mizutani, M. Katsuki, and T. Tabata, "Structure of Spark-Ignited Spherical Flames Propagating in a Droplet Cloud," in Developments in Laser Techniques and Applications to Fluid Mechanics, R. J. Adrian, Ed. Berlin: Springer-Verlag, 1996, pp. 212-223.
[9] H. F. Coward and F. Brinsley, "Dilution Limits of Inflammability of Gaseous Mixtures," Journal of Chemical Society Transaction (London), vol. 105, pp. 1859-1885, 1914.
[10] O. C. d. C. Ellis, "Flame Movements in Gaseous Mixtures," Fuel, vol. 7, pp. 195-205, 1928.
[11] I. Liebman, J. Corry, and H. E. Perlee, "Dynamics of Flame Propagation through Layered Methane-Air Mixtures," Combustion Science and Technology, vol. 2, pp. 365, 1971.
[12] G. E. Andrews and D. Bradley, "Limits of Flammability and Natural Convection for Methane-Air Mixtures," 14th Symposium (International) on Combustion, 1973.
[13] G. E. Andrews and D. Bradley, "Determination of Burning Velocities, A Critical Review," Combustion and Flame, vol. 18, pp. 133-153, 1972.
[14] D. Bradley, Personal Communications, 2006.
[15] C. T. R. Wilson, "Condensation of water vapour in the presence of dust-free air and other gases," Proc. of the Royal Society of London, 1897.
[16] D. Bradley, P. H. Gaskell, and X. J. Gu, "Burning Velocities, Markstein Lengths and Flame Quenching for Spherical Methane-Air Flames: A Computational Study," Combustion and Flame, vol. 104, pp. 176-198, 1996.
[17] F. Atzler, M. Lawes, S. A. Sulaiman, and R. Woolley, "Effects of Droplets on the Flame speeds of Laminar Iso-Octane and Air Aerosols," ICLASS 2006, Kyoto, Japan, 2006.
[18] F. Atzler, "Fundamental Studies of Aerosol Combustion," Department of Mechanical Engineering, University of Leeds, 1999.

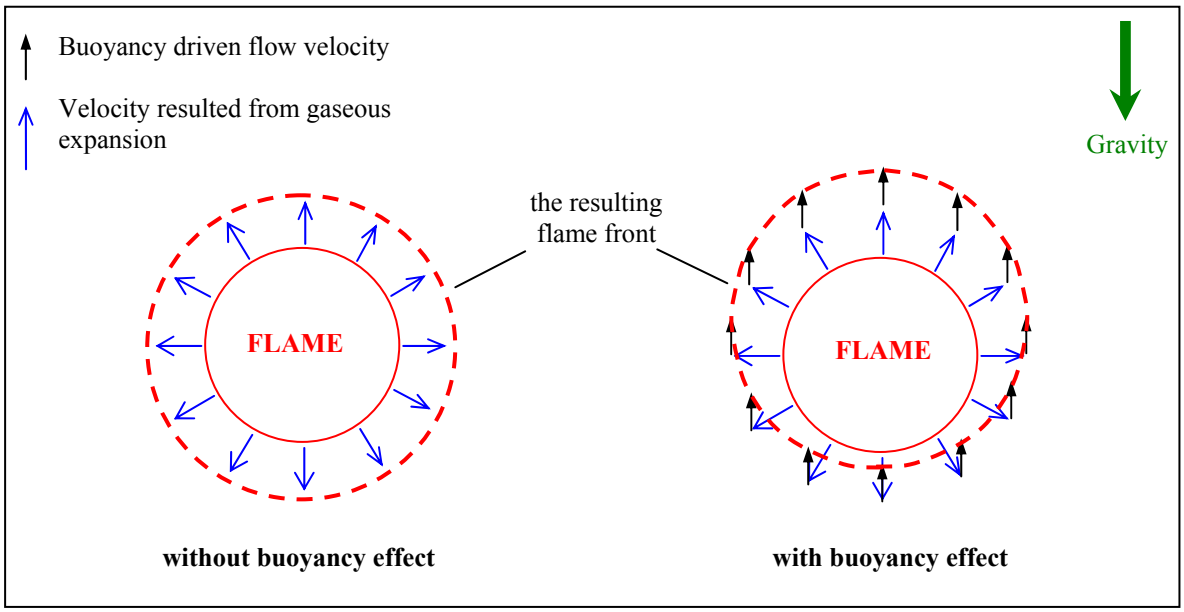

Fig. 1. Illustration of the buoyancy effect [14] on spherical flames. The arrows indicate the local velocities resulted by gas expansion and buoyancy driven convection

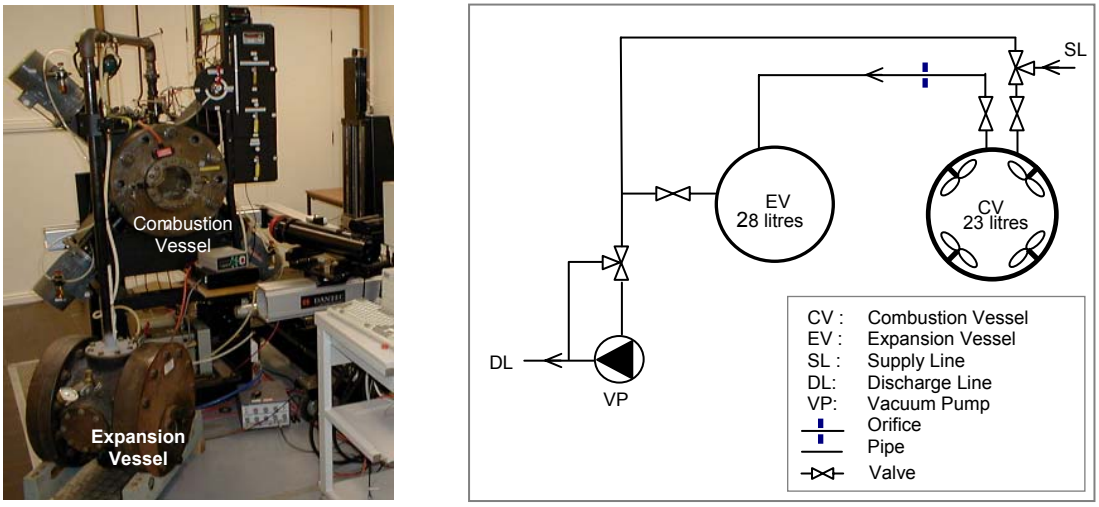

(a) (b)

Fig. 2. Aerosol combustion apparatus: (a) photograph (b) schematic

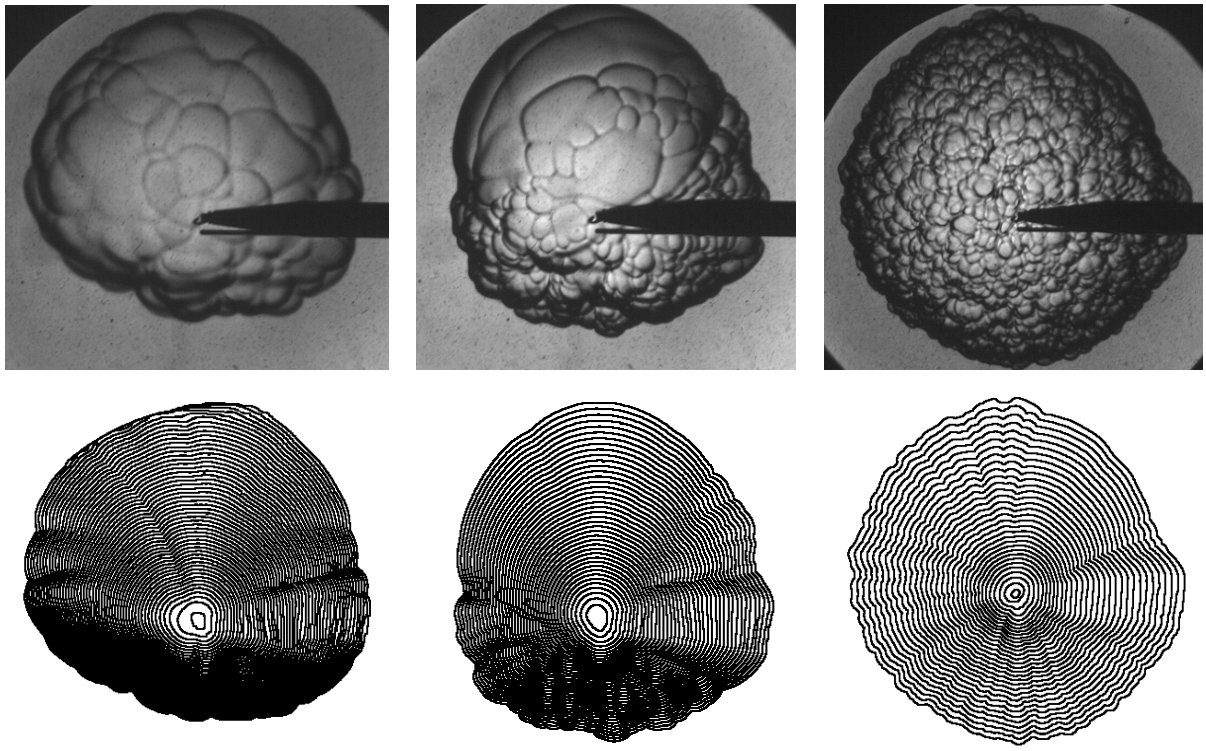

(a) D_{10} = 0μm (gaseous) (b) D_{10} = 5 μm (c) D_{10} = 13 μm

Fig. 3. Schlieren images and contour plots (superimposition of edges) throughout propagation for iso-octane-air flames at ϕ_{ov} = 2.0 and various droplet sizes. The time interval between each contour is 2 ms

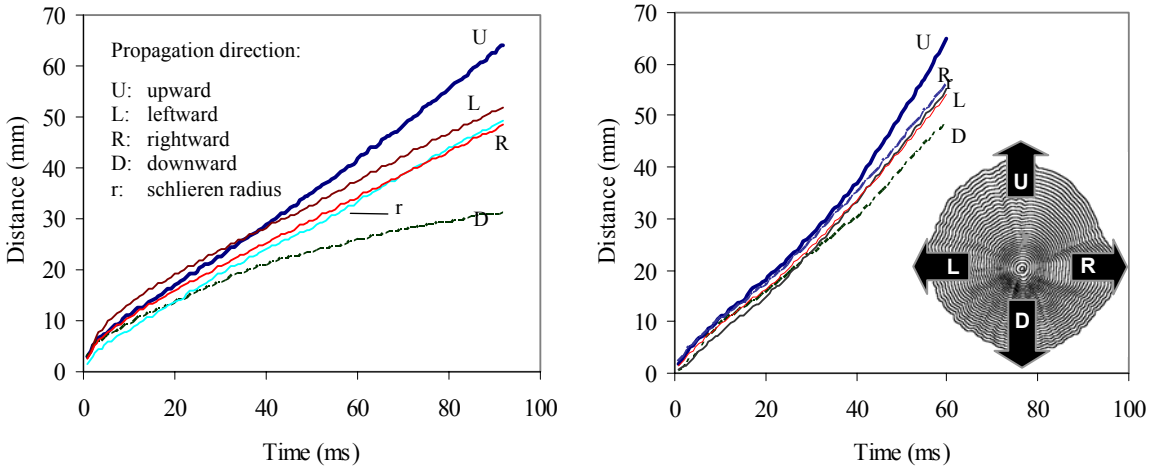

(a) gaseous, D_{10} = 0 μm (b) aerosol, D_{10} = 13μm.

Fig. 4. Flame propagation distance from spark electrode as a function of time for iso-octane-air mixtures at ϕ_{ov} = 2.0. Also shown is the corresponding direction of the flame propagation with respect to the spark electrode

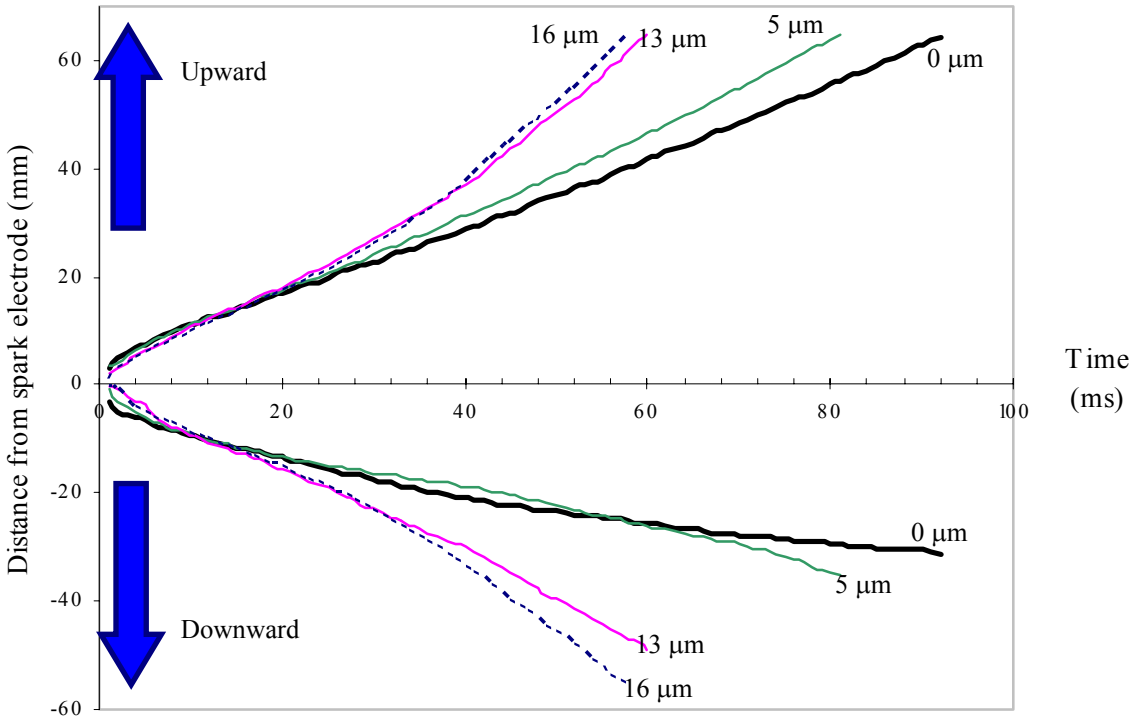

Fig. 5. Comparison of vertical flame propagation distance from spark electrode as a function of time for iso-octane-air mixtures at ϕ_{ov} = 2.0. Negative distances indicate downward flame propagation

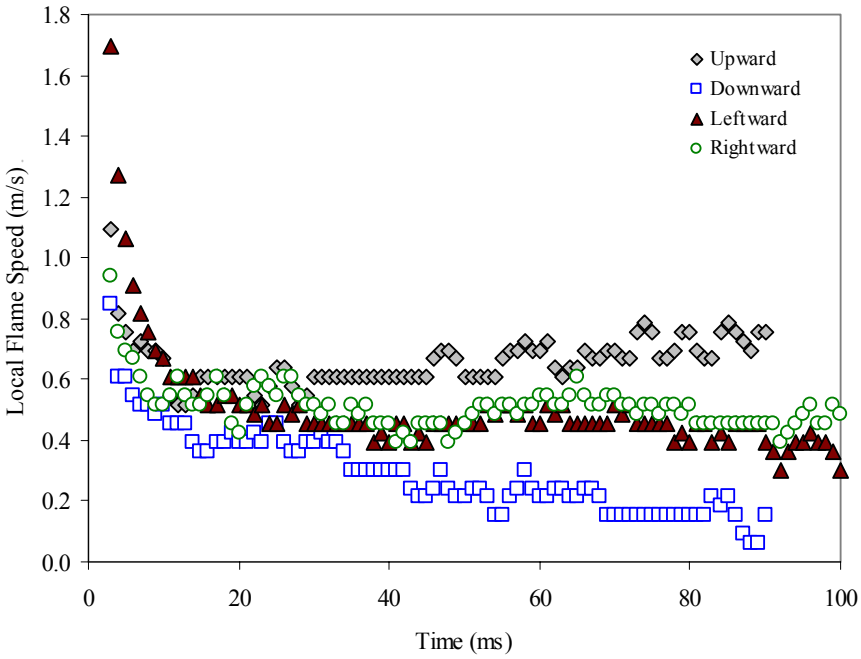

(a) gaseous, D_{10} = 0μm

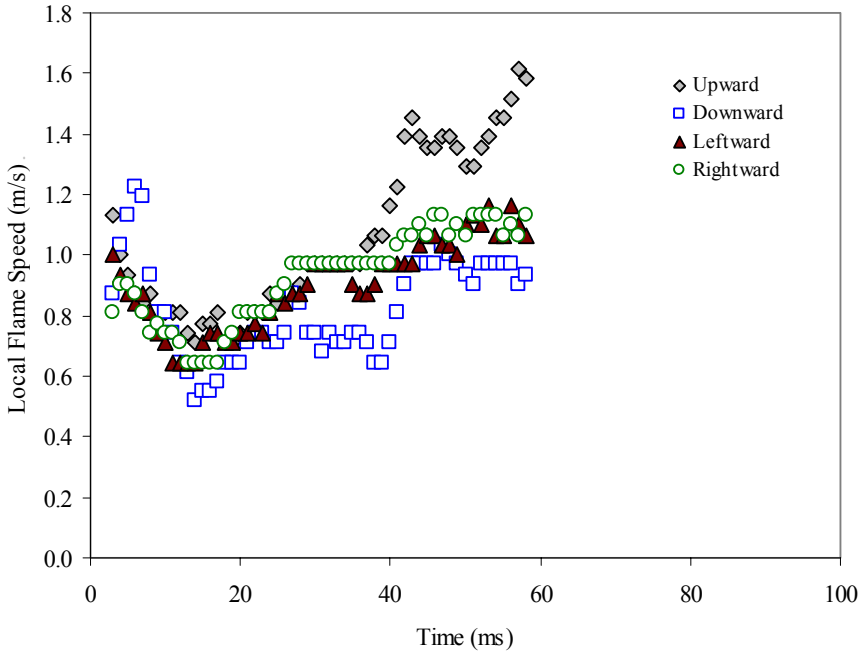

(b) aerosol, D_{10} = 13μm.

Fig. 6. Comparison of vertical flame propagation distance from spark electrode as a function of time air for iso-octane-air mixtures at ϕ_{ov} = 2.0 for (a) D_{10} = 0μm (gaseous) and (b) D_{10} = 13μm